Aerospace Science and Technology 14 (2010) 348–355

Contents lists available at ScienceDirect

Aerospace Science and Technology

www.elsevier.com/locate/aescte

Hybrid propulsion system for formation flying using electrostatic forces

C.M. Saaj [a,*], V. Lappas [a], H. Schaub [b], D. Izzo [c]

[a] Surrey Space Centre, University of Surrey, Surrey GU2 7XH, UK
[b] Aerospace Engineering and Sciences Department, University of Colorado, Boulder, CO 80309, USA
[c] Advanced Concepts Team, ESTEC, 2200 AG Noordwijk, The Netherlands

ARTICLE INFO

Article history:
Received 10 January 2007
Received in revised form 12 February 2010
Accepted 18 February 2010
Available online 19 March 2010

Keywords:
Coulomb force
Hybrid propulsion
Formation flying
Artificial potential field
Sliding mode control

ABSTRACT

Propulsion, path planning and control of spacecraft formations in Geostationary Earth Orbit (GEO) and other high Earth orbits present significant challenges to engineers. An innovative hybrid propulsion system for close-proximity (<50 m) formation flying is presented using electrostatic forces and standard electric/ion thrusters. The Sliding Mode Control (SMC) strategy generates the required inter-spacecraft forces based on the equivalent product of spacecraft surface charges. Collision-free aggregation and formation is realized using the Artificial Potential Field (APF) method. Simulation is performed to prove the efficacy of the proposed control, path planning and hybrid actuation schemes for close-proximity spacecraft formation flying in GEO and other high Earth orbits.

1. Introduction

In GEO and other high Earth orbits, spacecraft surface charging due to interaction with the plasma environment poses a major challenge. The literature on spacecraft charging is extensive, presented in [4,13,8,5,29]. Garett [4] reviewed the field of spacecraft surface charging in 1981. A detailed discussion of the space plasma environment can be found in the work of Hasting and Garret [13]. Although plasma physics has been studied for decades, formation flying is a relatively recent concept for space applications. Walker [31] explored the formation-flying concept in early 1980's. A few examples of successful real missions are: EO-1 in formation with LandSat-7, Cluster and ST-5. The main advantage of formation flying is that the functionality of one big spacecraft can be distributed among several small, low cost spacecraft working in co-operation thereby reducing the total mission cost.

Spacecraft in formation require propulsion systems in the range of micro-Newton to milli-Newton thrust levels. A range of propulsion technologies has been proposed with some emphasis on electric propulsion such as Pulsed Plasma Thrusters (PPT) and Field Emission Electric Propulsion [10,27,19]. A disadvantage for most propulsion techniques in close-proximity missions is the possibility that the propellant emitted will impinge upon neighboring spacecraft and damage or contaminate payloads.

In recent years, there has been much interest in close-proximity spacecraft formation flying. The spacecraft formation-flying concept exploiting the inter-spacecraft electrostatic force can be found in [16,26]. By generating different charges on spacecraft in close proximity, each spacecraft exerts a force on all the other spacecraft. This force can potentially be exploited to control the relative motion of the spacecraft [28]. More details on the concept of Coulomb Spacecraft Formations (CSF) can be found in [14,2,22,25,17]. In [14], Joe et al. used the principle of electrostatic forces to control the relative motion of a spacecraft formation. Berryman and Schaub [2] developed an algorithm to determine the steady state equilibrium in which the sum of acceleration on each spacecraft in the formation is zero. With Coulomb control, all forces are internal to the system, which means that the inertial linear and rotational momentum cannot be altered by Coulomb forces [22,25]. Use of Coulomb forces can allow the relative motion of spacecraft to be controlled without any contaminations which is a significant advantage compared to other propulsion techniques especially when one considers docking and close proximity maneuvers [17]. According to Garrett and Whittlesey [5], Coulomb forces of the order of 10–1000 μN can be produced on short timescales with less than 1 Watt of on-board power which is comparable with that produced by conventional electric thrusters. This makes Coulomb forces an attractive means of propulsion for small satellites where mass and power are significantly constrained.

Formation flying requires an intelligent path planning strategy in order to avoid spacecraft collisions. Many collision avoidance and path planning techniques have been researched for space and terrestrial applications. A well-known approach to collision-free path planning of terrestrial robots is using the APF method presented by Khatib [15]. Gazi [6] implemented an APF method for a multi-agent system or swarms. An artificial potential field based

* Corresponding author. Tel.: +44 1483682255.
E-mail address: C.Saaj@surrey.ac.uk (C.M. Saaj).

1270-9638/$ – see front matter
doi:10.1016/j.ast.2010.02.009

approach for autonomous spacecraft navigation and self-assembly in space can be found in [20,21]. Kong [18] considered the operation of multi-spacecraft systems in three different potential fields such that spacecraft formation can be held with as little effort as possible.

Spacecraft path planning would be successful only if the system is equipped with an efficient control system. Ayre et al. [1] developed a control scheme based on behavior-based control suitable for self-assembly and formation flying applications. Variable structure control with a sliding mode, first described in [3], laid out a well-described robust control method. Today, SMC is used as a general control method and is being examined for a wide spectrum of systems including nonlinear systems, multi-input/multi-output systems, discrete-time models, large scale and infinite-dimensional systems and stochastic systems. Numerous theoretical advances and practical applications have been reported in [30,9,32,24]. The methodology of using artificial potential field and sliding mode control for swarm aggregation and formation acquisition can be found in [6,7]. However, the benefit of sliding mode control has not yet been fully utilized for space applications. Izzo and Pettazzi [11,12] have developed a technique for satellite path planning that exploits a behavior-based approach to achieve an autonomous and distributed control of identical spacecraft over their relative geometry. Also it is proved that sliding mode control for satellite formation control is an effective way of implementing distributed architectures.

In this paper, a novel hybrid propulsion system is investigated for spacecraft formation flying utilizing Coulomb forces and electric/ion thrusters. Charge control strategies to control the relative motion of N satellites are still an active area of research. In particular, the required inter-spacecraft forces or equivalent product of spacecraft charges needs to be determined. A critical element in Coulomb forces is how to effectively map the charge products into individual spacecraft charges which is still an open challenge. To analyze the performance of the proposed hybrid approach, a strategy is devised based on using the charge products themselves to estimate the required power and resulting Coulomb forces. This approach does not involve the use of challenging nonlinear, analytic formulations of multiple spacecraft charges.

Having established a framework to estimate charge products for Coulomb forces, the path planning and control algorithm for spacecraft formation flying is designed based on the APF method and sliding mode control developed by Gazi [6]. This method is computationally less expensive than global approaches and provides a simple but effective path planner for real-time applications. The outline of the paper is as follows: A brief overview on Coulomb spacecraft charging and artificial potential field method is presented in Section 2. The new hybrid propulsion system and the proposed path planning and control architecture are explained in Section 3. The results of a simulation study for a tetrahedron formation are presented in Section 4, followed by the conclusions in Section 5.

2. Fundamentals

2.1. Coulomb spacecraft charging

Consider a close formation with N spacecraft of individual mass m_i in GEO or high Earth orbits. A vector $\mathbf{x}_i$ will denote the position vector of ith spacecraft relative to the inertial center of the Earth. The magnitude of the Coulomb force between two satellites (assumed spheres) with charges q_i and q_j in a plasma field is given by:

$$\mathbf{F}_{ij} = k_c\left(q_i q_j/\mathbf{x}_{ji}^2\right)\exp(-\mathbf{x}_{ji}/\lambda_d),$$

where $x_{ji} = x_j - x_i$ is the relative position vector, λ_d is the Debye length and $k_c = (4\pi\varepsilon_o)^{-1} = 8.99\times 10^9\ \mathrm{N\,m^2/C^2}$ is a constant of proportionality that depends on ε_o, the permittivity of free space. Then the electric field $\mathbf{E}_i$ experienced by the ith spacecraft having charge q_i is given by [31]:

$$\mathbf{E}_i = k_c\sum_{j=1,\ j\neq i}^{N} q_j\left(\mathbf{x}_{ji}/|\mathbf{x}_{ji}|^3\right)\exp\left(-|\mathbf{x}_{ji}|/\lambda_d\right),$$

where $i \neq j$. The Coulomb force experienced by ith satellite is $\mathbf{F}_i = q_i\mathbf{E}_i$. At GEO, the average value of the Debye length is about 200 m and its effect is very small if the spacecraft fly dozens of meters apart. Hence assuming a standard inverse square gravitational attraction, the full nonlinear inertial equations of motion of the ith spacecraft is given by:

$$\ddot{\mathbf{x}}_i + \left(\mu/\mathbf{x}_i^3\right)\mathbf{x}_i = (1/m_i)\sum_{j=1}^{N}\mathbf{F}_{ij},\quad i\neq j,$$

where μ is the Earth's gravitational constant.

2.2. Path planning using artificial potential field method

Let the formation consists of N individual agents (here spacecraft) in the n-dimensional Euclidean space [6]. The position of the ith agent is described by $\mathbf{x}_i \in \mathbf{R}^n$. It is assumed that synchronous motion exists and there is no time delay. The motion of each agent in the formation is governed by the equation:

$$\dot{\mathbf{x}}_i = \sum_{j=1,\, j\neq i}^{N} g(\mathbf{x}_i - \mathbf{x}_j),\quad i = 1,\ldots,N, \tag{1}$$

where $g(.)$ is an odd function which represents the sum of the function of attraction and repulsion between the agents. The function $g(.)$ can be represented by $g(\mathbf{y}) = -\mathbf{y}[g_a(\|\mathbf{y}\|) - g_r(\|\mathbf{y}\|)]$ where $\mathbf{y}\in\mathbf{R}^n$ is arbitrary and $\|\mathbf{y}\| = \mathrm{sqrt}(\mathbf{y}^T\mathbf{y})$ is the Euclidean norm. Eq. (1) can be represented also by:

$$\dot{\mathbf{x}}_i = -\nabla_{x_i}\mathbf{J}(\mathbf{x}),\quad i = 1,\ldots,N, \tag{2}$$

where $\mathbf{x}^T = [\,\mathbf{x}_1^T \quad \ldots \quad \mathbf{x}_N^T\,]$ is the lumped vector of the positions of all the agents and $\mathbf{J}:\mathbf{R}^{nN}\to\mathbf{R}$ is a potential function that represents the inter-agent interactions. The potential function $\mathbf{J}(\mathbf{x})$ depends on the relative positions of the agents in the formation. Under certain conditions, the above model results in aggregation of the agents [6]. In particular, it is needed that the attraction term $g_a(\|\mathbf{y}\|)$ dominates on large distances (needed for aggregation) and the repulsion term $g_r(\|\mathbf{y}\|)$ dominates on short distances (needed to avoid collisions) and there is a distance δ at which the attraction and the repulsion balance and $g_a(\delta) = g_r(\delta)$. Since there are no stochastics in the above model, it is inferred that given the initial positions of the agents $\mathbf{x}_i(0), i = 1,\ldots,N$, the final configuration to which the agents will converge is unique. However, in general it is difficult to find a direct relation between $\mathbf{x}(0)$ and the final position $\mathbf{x}(\infty)$. This is a shortcoming of the above model in which all the agents interact with all the other agents in the same manner and there are no pair-dependent relationships. Therefore, the above model is more for general aggregation purposes instead of formation control.

For formation control, one needs to achieve and maintain a predefined geometrical shape (a formation) from possibly arbitrary initial positions of the agents. For this reason, the above equation needs to be modified for formation control. Using the assumptions

on the potential function stated in [6,7], the equation of motion in (1) with the pair-dependent attraction/repulsion becomes:

$$\dot{\mathbf{x}}_i = \sum_{j=1,\, j\neq i}^{N} g_{ij}(\mathbf{x}_i - \mathbf{x}_j), \quad i = 1, \ldots, N, \tag{3}$$

where the attraction/repulsion function $g_{ij}(.)$ for all pairs (i, j) are odd functions and satisfy $g_{ij}(\mathbf{x}_i - \mathbf{x}_j) = -g_{ji}(\mathbf{x}_j - \mathbf{x}_i)$. For formation control, the attraction and repulsion functions, and therefore the equilibrium distances at which the attraction and the repulsion balance δ_{ij}, for different pairs of spacecraft can be different. In other words, for each pair (i, j) there is a distance δ_{ij} such that $g^a_{ij}(\delta_{ij}) = g^r_{ij}(\delta_{ij})$ (where $g^a_{ij}(\cdot)$ represents the pair-dependent attraction and $g^r_{ij}(\cdot)$ represents the pair-dependent repulsion) and depending on the formation requirements, it is possible to have $\delta_{ij} \neq \delta_{ik}$ for $k \neq j$.

The desired formation can be uniquely specified with respect to rotation and translation by the formation constraints $\|\mathbf{x}_i - \mathbf{x}_j\| = d_{ij}$ for all $(i, j), j \neq i$. The idea is to choose each of the attraction/repulsion functions $g_{ij}(.)$ such that $\delta_{ij} = d_{ij}$ for every pair of spacecraft (i, j). Then the corresponding potential function (or basically the generalized Lyapunov function)

$$\mathbf{J}(\mathbf{x}) = \sum_{i=1}^{N-1} \sum_{j=i+1}^{N} \left[\mathbf{J}_a^{ij}\left(\left\|\mathbf{x}^i - \mathbf{x}^j\right\|\right) - \mathbf{J}_r^{ij}\left(\left\|\mathbf{x}^i - \mathbf{x}^j\right\|\right)\right] \tag{4}$$

has its minimum at the desired formation and once the formation is achieved $\dot{\mathbf{x}}_i = 0$, $\forall i$. One issue to note here is that this type of potential suffers from local minima problem. However, the procedure based on the sliding mode control method discussed in the following section is not limited to this type of potentials only. In particular, if $\mathbf{J}(\mathbf{x})$ is chosen such that it has a unique minimum at the desired formation, then the desired formation will be asymptotically achieved for any initial condition. In the case of potentials with multiple local minima it is still guaranteed that the desired formation will be achieved, however this guarantee holds only locally.

3. Hybrid propulsion for spacecraft formation flying

3.1. Analysis of hybrid propulsion using electrostatic forces

This section presents the development of a strategy to investigate the effectiveness of the novel hybrid propulsion system that would take advantage of the naturally available electrostatic forces and thereby minimize the use of electric or ion propulsion. For example, the cluster internal Coulomb forces cannot change the inertial momentum of the formation. Thus, any navigation strategy that requires external forces on the formation cannot be implemented with a purely Coulomb-based control concept. Of interest is how well these APF-based control force can be implemented with Coulomb thrusting, and what forces components must be provided with Electric Propulsion (EP) systems. Some of the critical questions to be answered for the Coulomb thrusting involve power, charge management, sensing, and actuation strategies within the physical constraints of a small satellite. To determine an upper bound on the expected hybrid performance, it is assumed that the charge products can be perfectly implemented into individual real spacecraft charges. Future work will consider specific charge implementation techniques such as pulse-width modulation methods, or an integrated swarm navigation and charge selection technique.

Consider a formation of N spacecraft having $p = (N(N-1)/2)$ charge products. For example, for $N = 4$ there are six charge products i.e.,

$$\mathbf{Q} = [\, Q_{12} \quad Q_{13} \quad Q_{14} \quad Q_{23} \quad Q_{24} \quad Q_{34} \,]^T.$$

For the ith spacecraft, consider all possible pairs of charge product due to the remaining $N-1$ spacecraft as $Q_{ij} = q_i q_j$, $j = 1, \ldots, N, i \neq j$. Then the commanded force acting on ith spacecraft is:

$$\mathbf{F}_{ci} = \sum_{j=1, i\neq j}^{N} \left(k_c Q_{ij}/\mathbf{x}_{ji}^2\right)\mathbf{x}_{ij} \exp(-\mathbf{x}_{ji}/\lambda_d). \tag{5}$$

The commanded forces are obtained from the APF navigation strategy. At present this control logic makes no consideration for what forces are feasible with Coulomb thrusting and which are not. Rewriting Eq. (5) gives: $\mathbf{F}_{ci} = [\mathbf{A}_i][\tilde{\mathbf{Q}}]$, where

$$[\mathbf{A}_i] = \left[\left(k_c/x_{i1}^2\right)x_{i1}\exp(x_{i1}/\lambda_d) \quad \ldots \quad \left(k_c/x_{iN}^2\right)x_{iN}\exp(x_{iN}/\lambda_d)\right];$$

$$[\tilde{\mathbf{Q}}] = [\, q_i q_j \quad \ldots \quad q_i q_N \,]^T.$$

Then using the least-square inverse, $\tilde{\mathbf{Q}} = (\mathbf{A}_i^T\mathbf{A}_i)^{-1}\mathbf{A}_i^T\mathbf{F}_{ci}$ vector is determined. This represents the smallest set of charge products, which will come closest to producing the required commanded force. Thus the charge product $\tilde{\mathbf{Q}}$ for ith spacecraft is derived from its commanded force $\mathbf{F}_{ci}$. The charge product thus derived is then used for computing the actual thrust developed by Coulomb charging of ith spacecraft as:

$$\mathbf{F}_{CSFi} = [\mathbf{A}_i][\tilde{\mathbf{Q}}]. \tag{6}$$

Note that this actual Coulomb force will generally not be equal to the commanded force. The formation internal forces cannot change the cluster momentum. Such force components are produced by the Electric Propulsion (EP) system by computing:

$$\mathbf{F}_{EPi} = \mathbf{F}_{ci} - \mathbf{F}_{CSFi}. \tag{7}$$

From Eq. (7) it can be seen that the electric thrusters are used only for compensating the difference between the commanded force and that generated by electrostatic forces. For scenarios where the Coulomb force is saturated due to large separation distances, or because the inertial cluster momentum must be changed, the EP thrusting will smoothly compensate and guarantee that the required navigation control force is always produced.

The performance of Coulomb spacecraft charging is analyzed using the CSF parameters such as average power, peak power, specific impulse, mass flow rate, charge history and voltage on the spacecraft. Let $\mathbf{F}_{ai}$ denote the actual force available from the hybrid thrusters for the ith spacecraft for changing its maneuver. Due to the actuator dynamics, $\mathbf{F}_{ai}$ will differ in magnitude from the commanded thrust $\mathbf{F}_{ci}$. For simulation purposes, first, the charge product is determined from the commanded force $\mathbf{F}_{ci}$, and then $\mathbf{F}_{CSFi}$ and $\mathbf{F}_{EPi}$ are determined according to Eqs. (6) and (7) respectively. To estimate an upper performance bound of this hybrid control strategy, it is assumed that these charges can be perfectly implemented into individual N spacecraft charges. Next a set of formulae is developed based on the charge products to estimate the various Coulomb thrusting performance parameters:

1. Average cluster charge history $q_{hist} = \sum_i^N |\tilde{q}_i|/(N-1)$, where $\tilde{q}_i = \text{sqrt}(\tilde{\mathbf{Q}})$.
2. Using Gauss's law and assuming that the spacecraft is spherical with radius ρ, the surface potential is $V_{sci} = \tilde{q}_i/(4\pi\varepsilon_0\mathbf{x}_i)$ and the average spacecraft voltage is estimated as:
$$V_{sc} = \sum_{i=1}^{N}\left(\sum_{i=1}^{N}|V_{sci}|/(N-1)\right)\Big/(N).$$
3. CSF mass flow rate is $\dot{m} = I_e m_{ion}/(q_{ion})$, where I_e is the emission current, m_{ion} is the mass of ions and q_{ion} is charge of the ion. Then the average mass flow is $\dot{m}_{avg} = \sum(\sum\dot{m})/(p)$.

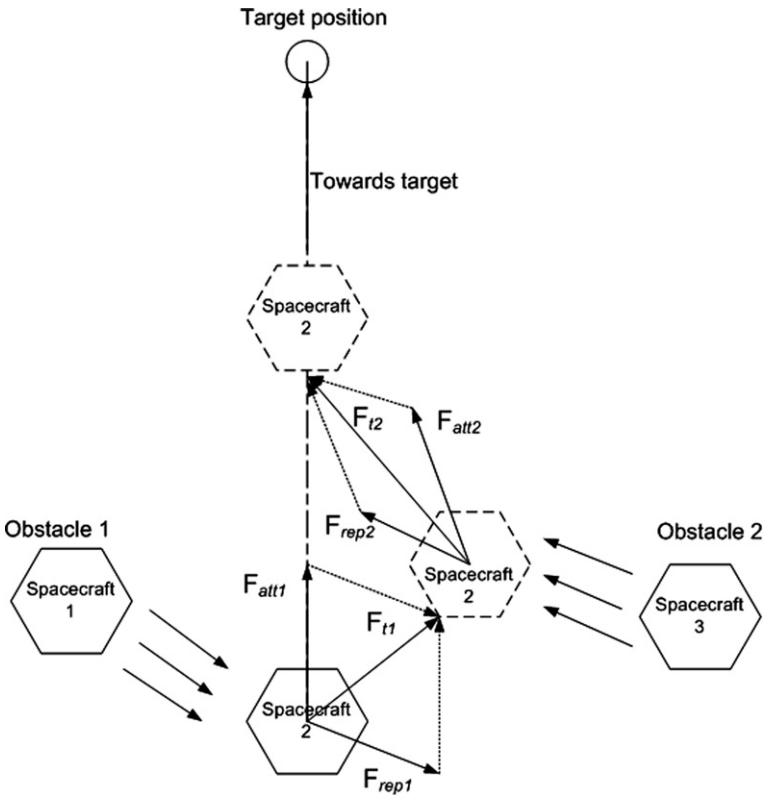

Fig. 1. Schematic diagram of spacecraft path planning using APF.

Note that first, all the mass flow rates of individual spacecraft for each pulse time, Δt_k is added and then averaged over t for p charge products.

4. The specific impulse $I_{sp} = \mathbf{F}_{CSF}/(\dot{m}_{avg} g_o)$, where $g_o = 9.81\ \mathrm{m/s^2}$.
5. Power generated due to Coulomb charging is $P_i = |V_{sc} I_e|$, where $|I_e| = 4\pi\varepsilon_o \rho^2 |J_p|$ is the emission current and J_p is the current density to the spacecraft from the plasma. The peak power is $P_{peak} = \max(\sum P_i/(N-1))$ and the average power is $P_{avg} = (\sum(\sum P_i/(N)))/(N-1)$.

3.2. Propulsion, path planning and control for spacecraft formation flying

In this section, the path planning and control algorithm for spacecraft formation flying is discussed based on the analysis of the APF method in Section 2.2 and Coulomb forces in Section 3.1.

Fig. 1 illustrates the force experienced by a spacecraft in a formation of three spacecraft using the APF method. It is required that 'spacecraft-2' moves towards the final target position. Initially, 'spacecraft-1' exerts a repulsive force, and the target exerts an attractive force on 'spacecraft-2'. Then it moves to a new location in the direction of the resultant force. At this position, 'spacecraft-3' exerts a repulsive force and target exerts an attractive force on 'spacecraft-2' and it moves towards the next intermittent location. Here the target exerts the attractive force and 'spacecraft-2' finally moves towards its target position, thereby achieving the desired configuration. In this approach, the steering direction of a particular spacecraft undergoing reconfiguration within the formation is determined by assuming that the other members of the formation (obstacles) assert repulsive forces on the spacecraft and the goal (desired terminal state) asserts attractive force. Consequently, the spacecraft experiences a generalized force equal to the negative of the total potential gradient that drives the spacecraft towards the goal or the desired terminal state. In this way the APF provides a constantly active navigation, offering a collision free trajectory for the each of the individual spacecraft that form part of a constellation or formation.

The schematic diagram of the proposed path planning, control and propulsion architecture is shown in Fig. 2. It integrates various sensory signals to achieve collision-free goal oriented aggregation and formation. The sliding mode controller commands the hybrid actuation system that is based on the electrostatic forces and electric/ion thrusters. The path-planning module is capable of avoiding obstacles and provides a goal-oriented navigation in an optimal time period. This approach has less computational load as compared to other techniques that carry out extensive map building from raw sensory data.

Consider the nonlinear inertial equation of motion of the spacecraft represented by:

$$\mathbf{M}_i(\mathbf{x}_i)\ddot{\mathbf{x}}_i + \mathbf{f}_i(\mathbf{x}_i, \dot{\mathbf{x}}_i) = \mathbf{F}_{ai}, \quad 1 \leqslant i \leqslant N, \tag{8}$$

where $\mathbf{x}_i \in \mathbf{R}^n$ is the position vector of spacecraft i, $\mathbf{M}_i \in \mathbf{R}^{n\times n}$ is the mass or inertia matrix and is assumed to be nonsingular, N is the number of spacecraft in the formation and $\mathbf{F}_{ai} \in \mathbf{R}^n$ is the control input. Here $\mathbf{F}_{ai}$ denote the actual force available from the hybrid thrusters to ith satellite for changing its maneuver. The additive term $\mathbf{f}_i(\mathbf{x}_i, \dot{\mathbf{x}}_i) \in \mathbf{R}^n$ is assumed to be of the form $\mathbf{f}_i(\mathbf{x}_i, \dot{\mathbf{x}}_i) = \mathbf{f}_i^k(\mathbf{x}_i, \dot{\mathbf{x}}_i) + \mathbf{f}_i^u(\mathbf{x}_i, \dot{\mathbf{x}}_i)$, where $\mathbf{f}_i^k(\mathbf{x}_i, \dot{\mathbf{x}}_i)$ represents the known part and $\mathbf{f}_i^u(\mathbf{x}_i, \dot{\mathbf{x}}_i)$ is the unknown part of the system dynamics. In the APF method, corresponding to (8), the motion of the individual spacecraft is governed by (3). For the sliding mode control method, the n-dimensional sliding manifold for ith spacecraft is chosen as:

$$\mathbf{s}_i = \dot{\mathbf{x}}_i + \nabla_{x_i}\mathbf{J}(\mathbf{x}) = 0, \quad i = 1, \ldots, N. \tag{9}$$

Note that here the potential function $\mathbf{J}(\mathbf{x})$ is not static. It depends on the relative positions of the individual spacecraft and need to satisfy certain assumptions made in [6]. Once all the spacecraft reach the respective sliding manifolds $\mathbf{s}_i = 0$, Eq. (9) reduces to

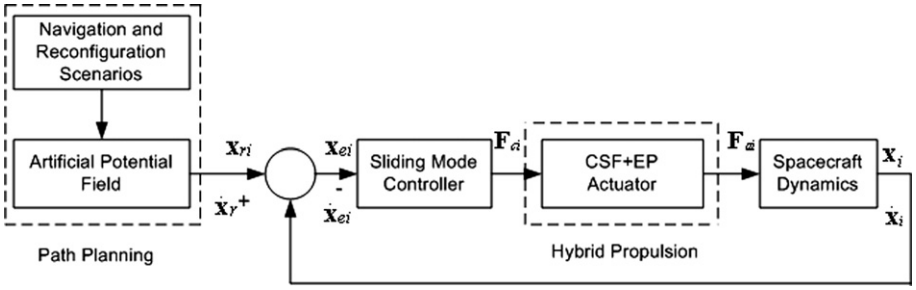

Fig. 2. Schematic diagram of spacecraft path planning, propulsion and control.

$\dot{\mathbf{x}}_i = -\nabla_{x_i}\mathbf{J}(\mathbf{x})$ which is same as the motion in (3). A sufficient condition for sliding mode to occur given in [3] is satisfaction of:

$$\mathbf{s}_i^T \dot{\mathbf{s}}_i < 0, \quad \forall i = 1, \ldots, N. \tag{10}$$

This guarantees that starting from any initial point in the state space; the sliding manifold is reached asymptotically. Further, if the condition $\mathbf{s}_i^T \dot{\mathbf{s}}_i < -\varepsilon\|\mathbf{s}_i\|$, $\forall i = 1, \ldots, N$ is satisfied, then it is guaranteed that sliding mode will occur in finite time. In order to achieve this objective, the sliding mode controller is given by:

$$\mathbf{F}_{ci} = -\mathbf{F}_{oi}\,\mathrm{sign}(\mathbf{s}_i) + \mathbf{f}_i^k(\mathbf{x}_i, \dot{\mathbf{x}}_i), \tag{11}$$

where $\mathrm{sign}(\mathbf{s}_i) = [\,\mathrm{sign}(\mathbf{s}_1) \quad \ldots \quad \mathrm{sign}(\mathbf{s}_N)\,]^T$. The gain of the control input is chosen as $\mathbf{F}_{oi} > (1/\underline{M}_i)(\overline{M}_i \bar{f}_i + \bar{J} + \varepsilon_i)$, for some $\varepsilon_i > 0$, and (with this choice) it is guaranteed that $\mathbf{s}_i^T \dot{\mathbf{s}}_i < -\varepsilon_i\|\mathbf{s}_i\|$. In the above controller, only the known part $\mathbf{f}_i^k(\mathbf{x}_i, \dot{\mathbf{x}}_i)$ of the disturbance is considered. Here $\underline{M}_i$ and $\overline{M}_i$ are the known lower and upper bounds of the inertia matrix/mass of the spacecraft respectively. Note that individual agents with point mass dynamics with uncertainties are considered for the sliding mode controller design in [6].

For practical implementations, a major inherent drawback of sliding mode controller is the chattering phenomenon. Finite high frequency oscillations are generated due to the presence of unmodeled fast dynamics of the sensors and actuators and due to nonideal realization of the relay characteristics of the SMC. In order to reduce the chattering phenomenon, the $\mathrm{sign}(\mathbf{s}_i)$ term in the controller equation (11) can be replaced by a smooth approximation using $\tanh(\beta\mathbf{s}_i)$. Note that this smoothing function does not guarantee full chatter elimination. It only ensures that the resulting sliding motion will lie in a close vicinity of the sliding manifold. An advanced chattering elimination techniques is using the higher order sliding mode control. However, discussion on chatter elimination techniques is beyond of the scope of this paper. The sliding mode controller used in this study is:

$$\mathbf{F}_{ci} = -\mathbf{F}_{oi}\tanh(\beta\mathbf{s}_i) + \mathbf{f}_i^k(\mathbf{x}_i, \dot{\mathbf{x}}_i). \tag{12}$$

Note that this controller is designed following the procedure in [6] and as if there is no actuator in the system. In other words, it is designed as if the control variable $\mathbf{F}_{ci}$ in (12) is the control input $\mathbf{F}_{ai}$ in Eq. (8). However, here the dynamics of the hybrid propulsion actuator are present as well and since they are not considered during the design of the controller (basically they are unmodeled dynamics) they may have negative effect on the performance of the system. The proposed path planning and control strategy will have all the benefits associated with the APF method and SMC along with the added advantage of utilizing Coulomb forces.

4. Results and discussion

A 3-dimensional formation flying scenario is used to showcase the benefits of the proposed hybrid propulsion system, collision avoidance strategy and sliding mode controller. The Snecma PPS 1350 EP thruster was selected for the simulation study. The Snecma PPS 1350 EP thruster was successfully flown on-board the European Space Agency's Smart-1 lunar probe. Moreover, this electric thruster is suitable for operating over 5000 hours and has stable operation over a power range of 1200 W to 1600 W. Moreover, the starting power requirement is also low and it suits for the applications considered in this work. The characteristics of the thruster are shown in Table 1.

Table 1
Snecma PPS 1350 thruster specifications.

Features	Value/units
Power (nominal)	1500 W
Thrust (peak)	88 mN
Specific Impulse	1650 sec
Mass	5.3 kg
Supply voltage	350 V
Efficiency	55%

Table 2
CSF simulation parameters.

Spacecraft parameter	Value/units
Spacecraft mass	150 kg
Bounds on mass	±50%
Radius	0.5 m
Debye length	200 m
Charge saturation limit	2 μC
Number of spacecraft	4
Maximum initial separation	5 km
Manoeuvre time	24 hrs
Peak magnitude of differential disturbance	2 μN
Final formation separation	50 m

Consider the nonlinear inertial model in Eq. (8). The effect of gravity and other orbit dynamics are neglected for simulation purposes. The spacecraft is assumed to be floating freely in GEO. However, a representative and slowly time varying (24 hour period) differential solar radiation perturbation with a 2 micro-Newton magnitude is included in the simulation in order to make the simulation more realistic. Such small disturbances for very close cluster formation flying can cause a notable deviation over a 24-hour time period.

The simulation parameters are shown in Table 2. The Coulomb spacecraft formation is illustrated using four spacecraft forming a tetrahedron formation, although the algorithm can be extended for any number of spacecraft. The initial conditions of the spacecraft are randomly chosen such that the initial, average inter-spacecraft separation is around 50 m and the initial velocity is assumed to be zero. The worst case disturbance is modeled based on the work of Romanelli et al. [23], who studied the effects of worst-case differential orbital perturbations on the motion of close flying spacecraft in GEO. For simulation purposes, choose $N = 4, n = 3, \varepsilon_i = 1, \bar{J} = 0.01$ N and $\bar{f}_i = 2$ μN. The differential solar radiation perturbation force acting on the system is chosen as

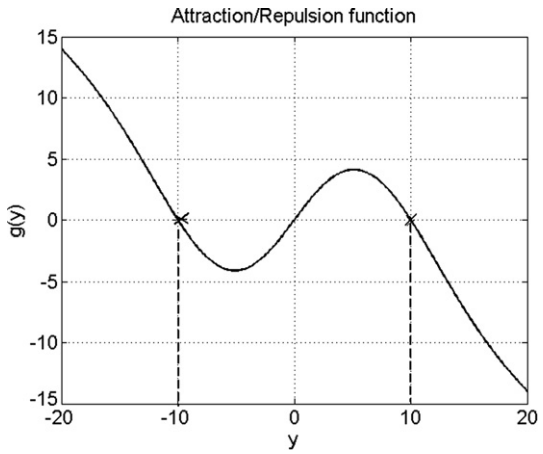

Fig. 3. Plot of the linear attraction and exponential repulsion function.

$\mathbf{f}_i^k(\mathbf{x}_i, \dot{\mathbf{x}}_i) = 2 \times 10^{-6} \sin(2(2\pi/t))$ N and it satisfies the assumption on the bound $\|\mathbf{f}_i^k(\mathbf{x}_i, \dot{\mathbf{x}}_i)\| = \|2 \times 10^{-6} \sin(0.2t)\| \leqslant 2 \times 10^{-6} \triangleq \bar{f}_i$.

The linear attraction and exponential repulsion type potential function developed in Gazi [7] is considered here and is given by:

$$g(y) = -y\big(a - b\exp\big(-\|y\|^2/c\big)\big),$$

where $a = b\exp(-d^2/c)$, $b = 5 \times 10^{-5}$, $c = 100$ and $d = 10$. The parameter a is computed in order to achieve the balance of attraction and repulsion between any two agents at the desired distance d in the final tetrahedron formation. By increasing the repulsive force (i.e. by increasing b) it is possible to guarantee collision avoidance.

From the plot of this potential function in Fig. 3, it can be seen that this function is attractive (i.e., a dominates) for large distances and repulsive (i.e., $b\exp(-(\|y\|^2/c))$ dominates) for small distances. The co-ordinates $(-10, 0)$ m and $(10, 0)$ m at which plot crosses the horizontal axis ($g(y) = 0$) constitute the desired formation separation of 10 m. The distance at which the attraction force balances the repulsion force is calculated as $\delta = \text{sqrt}(c/\ln(b/a)) = 10$ m.

The plots from the simulation for the tetrahedron formation are shown in Fig. 4. Fig. 4a shows the trajectories of the spacecraft from initial positions to the desired final positions. Circles represent the initial positions of the four spacecraft. The four spacecraft move to their desired inter-spacecraft separation of 10 m and form the required tetrahedron formation while avoiding collisions. Fig. 4b shows the final tetrahedron formation. Spheres represent the final positions after 24 hrs and the center of the formation is represented by '$*$'. The average distance of each spacecraft with respect to the formation center is calculated as $l_c = 10\,\text{sqrt}(3/8)$. During the transient phase, before the occurrence of the sliding mode it is possible for the center $\bar{x}$ to move. However, once the sliding mode occurs the center is expected to remain almost stationary. For practical implementation, there could be small deviations even after transient phase, which are due to chattering effects. Fig. 4c shows the minimum, average and the maximum distances between the individual spacecraft in the formation. The minimum, average and maximum inter-spacecraft distance after 24 hrs is 9.8 m, 10 m and 10.2 m respectively. It is observed that the average distance between spacecraft in the tetrahedron formation is equal to the side length of the tetrahedron or the final inter-spacecraft separation of 10 m. Figs. 5a and 5b show the average CSF power and potential respectively. The charge saturation limit is taken as 2 μC and the CSF specific impulse is shown in Fig. 5c. The commanded force $\mathbf{F}_{ci}$ from the sliding mode controller for all the four spacecraft in the formation is shown in Fig. 5d. The generated Coulomb force $\mathbf{F}_{CSFi}$ and the EP thrust $\mathbf{F}_{EP}$ are shown in Figs. 5e and 5f respectively. These results illustrate that the thrust generated by Coulomb force reduces the use of electric propulsion for close-proximity formation flying missions.

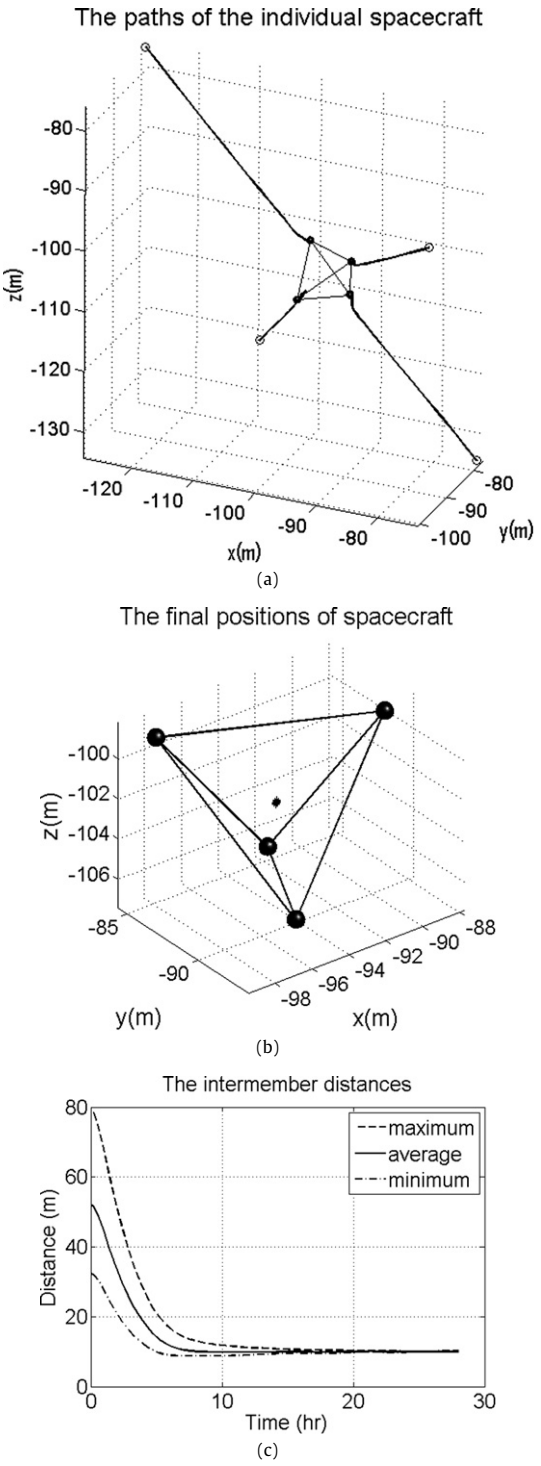

Fig. 4. Simulation plots for tetrahedron formation: Path planning (a)–(c).

5. Conclusions

A novel hybrid propulsion system using Coulomb forces and electric/ion propulsion is developed for spacecraft formation flying in GEO and other high Earth orbits. A tetrahedron formation scenario is used to demonstrate the effectiveness of the hybrid propulsion technique. The APF method guarantees collision-free

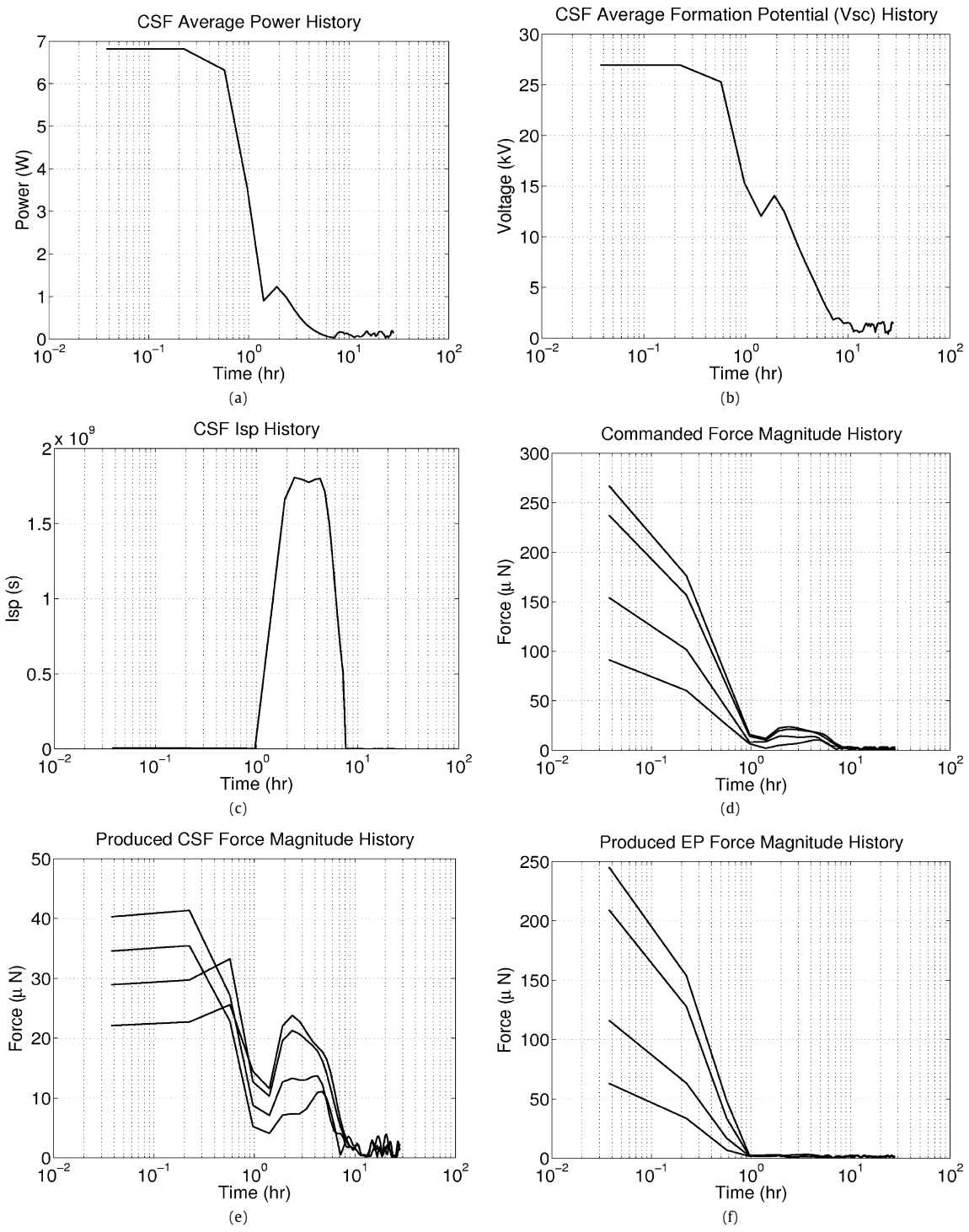

Fig. 5. Simulation plots for tetrahedron formation: Hybrid propulsion parameters (a)–(f).

aggregation. Since Sliding Mode Control guarantees robust performance, the impact of external perturbations like differential solar radiation and internal perturbations like change in mass due to fuel consumption will have negligible impact on the performance of the spacecraft. For the tetrahedron formation scenario considered in this study, the control effort is less due to the inherent robustness of the controller. This results in a fuel-efficient system for close-proximity formation flying missions.

Coulomb forces are used to control the relative motion between spacecraft when the separation distances are less than 50 m. For larger separation distances or for control forces, which do not lie along the line-of-sight vectors, electric thrusters are employed. The analysis conducted proves the effectiveness of the strategy using an estimate of the charge product with out having to use full charge feedback control. The general charge control of N spacecraft is still an active and open area of research. The charging product logic can be used for an N number of spacecraft without going into the complexities and nonlinearities of calculating the specific charges. This method, though still an estimate of charge products, is effective and important to show the feasibility of CSF and enables the system design of the overall hybrid propulsion system.

Acknowledgements

This project was funded by European Space Agency under contract No. 19697/06/NL/HE. We also like to express our thanks to Dr. Veysel Gazi (TOBB University of Economics and Technology, Turkey) for the fruitful and useful technical discussions.

References

[1] M. Ayre, D. Izzo, L. Pettazzi, Self assembly in space using behaviour based intelligent components, in: TAROS 2005, Towards Autonomous Robotic Systems, Imperial College, London, UK, 2005.
[2] J. Berryman, H. Schaub, Static equilibrium configurations in GEO Coulomb spacecraft formations, in: AAS Spaceflight Mechanics Meeting, Copper Mountain, CO, 2005, Paper No. 05-104.
[3] S.V. Emelyanov, Design of variable structure control systems with discontinuous switching functions, Engineering Cybernetics 1 (1964) 156–160.
[4] H.B. Garrett, The charging of spacecraft surfaces, Rev. Geophys. 19 (1981) 577–616.
[5] H.B. Garrett, A.C. Whittlesey, Spacecraft charging, an update, IEEE Transactions on Plasma Science 28 (6) (2000) 2017–2028.
[6] V. Gazi, Swarm aggregations using artificial potentials and sliding mode control, IEEE Transactions on Robotics 21 (6) (2005) 1208–1214.
[7] V. Gazi, K.M. Passino, A class of attraction/repulsion functions for stable swarm aggregations, International Journal of Control 77 (18/15) (2004) 1567–1579.
[8] D. Hasting, H. Garret, Spacecraft–Environment Interactions, Cambridge University Press, Cambridge, UK, 1996, pp. 44–71.
[9] B.S. Heck, A.A. Ferri, Application of output feedback to variable structure systems, Journal of Guidance, Control and Dynamics 12 (1989) 932–935.
[10] W.A. Hoskins, M.J. Wilson, N.J. Meckel, M. Campell, S. Chung, in: Proc. 35th AIAA/ASME/SAE/ASEE Joint Propulsion Conference, Los Angeles, CA, 1999.
[11] D. Izzo, L. Pettazzi, Equilibrium shaping: Distributed motion planning for satellite swarm, in: 8th International Symposium on Artificial Intelligence, Robotics and Automation in Space, Munich, Germany, 2005.
[12] D. Izzo, L. Pettazzi, Autonomous and distributed motion planning for satellite swarm, Journal of Guidance Control and Dynamics 30 (2) (2007) 449–459.
[13] B.F. James, O.W. Norton, M.B. Alexander, The natural space environment: Effects on spacecraft, NASA Reference Publication 1350, 1994.
[14] H. Joe, H. Schaub, G.G. Parker, Formation dynamics of Coulomb satellites, in: 6th Int. Conf. on Dynamics and Control of Systems and Structures in Space, Cinque Terre, Liguria, Italy, 2004.
[15] O. Khatib, Real-time obstacle avoidance for manipulator and mobile robots, The Int. J. Robotics Research 5 (1) (1986) 90–98.
[16] L.B. King, G.G. Parker, S. Deshmukh, J.H. Chong, Propellantless control of spacecraft swarms using Coulomb forces, NIAC Final Report, 2002.
[17] L.B. King, G.G. Parker, S. Deshmukh, J.H. Chong, Study of inter-spacecraft Coulomb forces and implications for formation flying, Journal of Propulsion and Power 19 (3) (2003) 497–505.
[18] E.M. Kong, Spacecraft formation flights exploiting potential fields, PhD Thesis, Department of Aeronautics and Astronautics, Massachusetts Institute of Technology, 2002.
[19] M. Martinez-Sanchez, J.E. Pollard, Spacecraft electric propulsion-an overview, J. Propulsion and Power 14 (5) (1998) 688–699.
[20] C.R. McInnes, Potential function methods for autonomous spacecraft and control, Paper No. AAS 95-447, 1995.
[21] F. McQuade, Autonomous control for on-orbit assembly using artificial potential functions, PhD Thesis, Faculty of Engineering, University of Glasgow, 1997.
[22] E.G. Mullen, M.S. Gussenhoven, D.A. Hardy, SCATHA survey of high-voltage spacecraft charging in sunlight, Journal of the Geophysical Sciences 91 (1986) 1074–1090.
[23] C.C. Romanelli, A. Natarajan, H. Schaub, G.G. Parker, L.B. King, Coulomb spacecraft voltage study due to differential orbital perturbations, in: AAS Space Flight Mechanics Meeting, Tampa Florida, January 22–26, 2006, Paper No. AAS 06-123.
[24] C.M. Saaj, B. Bandyopadhyay, H. Unbehauen, A new algorithm for discrete-time sliding mode control using fast output sampling feedback, IEEE Transactions on Industrial Electronics 49 (2002) 518–523.
[25] H. Schaub, M. Kim, Orbit element difference constraints for Coulomb satellite formations, in: AIAA/AAS Astrodynamics Specialist Conference, Providence, RI, 2004, Paper No. AIAA 04-5213.
[26] H. Schaub, G.G. Parker, L.B. King, Challenges and prospects of Coulomb spacecraft formations, in: AAS John L. Junkins Astrodynamics Symposium, College Station, TX, 2003, Paper No. AAS-03-278.
[27] M. Tajmar, J. Mitterauer, J. Wang, Field-emission-electric-propulsion (FEEP) plasma modeling: 3D full particle simulations, in: AIAA/ASME/SAE/ASEE Joint Propulsion Conference, Los Angeles, CA, June 20–24, 1999.
[28] K. Torkar, W. Riedler, C.P. Escoubet, R. Fehringer, R. Schmidt, R.J.L. Grard, H. Arends, F. Rudenauer, W. Steiger, B.T. Narheim, K. Svenes, R. Torbert, M. Andre, A. Fazakerley, R. Goldstein, R.C. Olsen, A. Pedersen, E. Whipple, H. Zhao, Active spacecraft potential control for cluster-implementation and first results, Annales Geophysicae 19 (2001) 1289–1302.
[29] A.C. Tribble, The Space Environment: Implications for Spacecraft Design, Princeton University Press, 2003.
[30] V.I. Utkin, Equations of the slipping regime in discontinuous systems: I, Automation and Remote Control 32 (1971) 1897–1907.
[31] J.G. Walker, The geometry of cluster orbits, J. Brit. Interplan. Soc. 35 (1982) 345.
[32] K.D. Young, V.I. Utkin, U. Ozguner, A control engineer's guide to sliding mode control, IEEE Transactions on Control Systems Technology 7 (3) (1999) 328–342.